CONFIGURATION EFFECTS ON SATELLITE CHARGING RESPONSE

C. K. Purvis

National Aeronautics and Space Administration
Lewis Research Center
Cleveland, Ohio 44135

Prepared for the
Eighteenth Aerospace Sciences Meeting
sponsored by the American Institute of Aeronautics and Astronautics Pasadena,
California, January 14-16, 1980

CONFIGURATION EFFECTS ON SATELLITE CHARGING RESPONSE

C.K. Purvis
National Aeronautics and Space Administration
Lewis Research Center
Cleveland, Ohio 44135

Abstract

A computer study of the response of various spacecraft configurations to a charging environment in sunlight using the NASCAP code is reported. Configuration features considered in the study include geometry, type of stabilization, and overall size. Results indicate that sunlight charging response is dominated by differential charging effects. Shaded insulation charges negatively resulting in the formation of potential barriers which suppress photoelectron emission from sunlit surfaces. Sunlight charging occurs relatively slowly: with 30 minutes of charging simulations, in none of the configurations modeled did the most negative surface cell reach half its equilibrium potential in eclipse. Because the substorm environment tends not to remain constant over long time periods (say 2l hr), this result implies that equilibrium calculations of spacecraft potentials in sunlight do not give an accurate indication of charging response in substorms.

Configuration features have an important impact on both charging rates of structures and on differential potentials developed across shaded insulators. The most striking "configuration" effect observed in this study is that of type of stabilization. A spinning spacecraft is expected to exhibit slower charging of its structure but to develop somewhat larger electric field stresses across shaded insulation than is an identical spacecraft which is three-axis stabilized. This effect, as well as those of other configuration features, are discussed. Data from the ATS-5 and ATS-6 spacecraft are presented, and support the analytical conclusions.

I. Introduction

The idea that spacecraft configuration is a critical factor in charging response was sparked by the observation that the ATS-5 and ATS-6 spacecraft respond similarly to charging environments in eclipse but differently in sunlight. Both space-craft charge negatively during substorm activity, which is consistent with the observation that ambient electron fluxes are larger than ambient ion fluxes. In the fall of 1974, when both spacecraft were eclipsed simultaneously, they charged to similar potentials.(1) Statistical analysis of ATS-5 and ATS-6 eclipse charging data(' further supports the conclusion that these two spacecraft exhibit similar charging response in eclipse. The factor of 2 difference in the most negative potential observed in eclipse (-10 kV for ATS-5, and -20 kV for ATS-6) is believed to be due to an in-crease in geometric activity between the ATS-5 and ATS-6 missions (2) rather than a difference in response to a given environment. The percentage of eclipse passages during which charging occurs is also similar for the two spacecraft.

In contrast, neither the frequency of charging nor the potentials attained by these spacecraft are similar in sunlight conditions. Reasoner, et al.(3)have studied daylight charging of ATS-6. They re-port a maximum negative potential of -2200 V and a "significant probability" of potentials more negative than -1000 V. They indicate a greater than 50% probability of charging in the midnight to dawn local time quadrant. Daylight charging of ATS-5 was discussed by DeForest, (4) who recorded 13 occurrences of charging to potentials more negative than -50 V lasting longer than 5 minutes between Sept. 30, 1969 and Nov. 10, 1970. The most negative potential observed was -300 V. Even allowing for a factor of 2 in geomagnetic activity, and for the in-ability of the ATS-5 detectors to record potentials less than 50 V in magnitude, it is apparent that ATS-6 charges more frequently and to larger negative potentials than does ATS-5.

The potentials discussed above are those of the spacecraft structures (electrical reference) with respect to plasma potential. For a spacecraft with electrically isolated surfaces (i.e., insulating surfaces), differential charging of these surfaces with respect to the spacecraft structure can occur because of differences in the surface materials' properties (such as secondary electron yield) and/or in the "environment" between surfaces (such as one surface being sunlit, and another shadowed). Potentials attained in eclipse in a given environment are determined by surface material properties. The fact that ATS-5 and ATS-6 charged to similar potentials in the same eclipse environment (1) suggests that the surface material properties which determine eclipse potential are similar for the two spacecraft. This implies that the dominant factors responsible for the very different behavior of the two spacecraft in sunlight is related to

differences in configuration rather than differences in materials. Configuration here includes characteristics such as size, geometry, and type of stabilization. These features determine relative areas of sunlit and shaded surfaces and are expected to be important for differential charging.

The differences in configuration between ATS-5 and ATS-6 are substantial, as indicated in figures 1 and 2 and table I. (5). ATS-5 is relatively small, compact, and spins at 76 rpm about the cylinder axis. ATS-6 is an extended object, five times as large and 3-axis stabilized. What should the effects of these various configuration features be on charging response, according to current understanding of the phenomena? Are these effects consistent with the observed response of ATS-5 and ATS-6? These are the two questions whose answers are sought in this study.

II. Study Approach

The approach chosen to answer the two questions posed above was to use the NASA Charging Analyzer Program (NASCAP) code(6) to investigate the effects of various configuration features on charging response, and to review data from the UCSD Auroral Particles experiments on ATS-5 and ATS-6 with particular attention to characteristic features of sun-light charging events.

For the NASCAP study, five objects were modeled. The configuration features examined were type of stabilization, geometry, and size. The environment was the same for all runs, and was an isotropic Maxwellian with electron temperature (kTe) = 5 keV, ion temperature (kTi) = 10 keV, and number densities of electrons and ions (ne and ni, respectively) = $0.2/cm^3$. To eliminate effects due to differing material properties, all materials were taken to have the same electron emission properties. Thus the effects examined are essentially sun/shade effects.

ATS-5 data from the first 2 years of operation (1969-1971) and ATS-6 data from 1974-1976 were re-viewed to identify sunlight charging response characteristics. Particular attention was focused on the temporal development of negative spacecraft potentials and on evidence of potential barriers (ATS-6) and differential charging (ATS-5). Frequency of charging was also tallied for ATS-5, for a comparison with the ATS-6 data discussed earlier.

III. NASCAP Study

A. Objects and Comparisons

The five NASCAP objects modeled for this study are illustrated in figures 3 to 7. Each figure shows a perspective view of an object (with a coordinate system for reference), indicates the exposed surface composition and gives a brief description of the object and size(s) and stabilization types run. A summary of comparisons made to identify the impact of stabilization type, size, and geometry appears in table II. All calculations were made for the plasma environment described above. Calculations were made for all objects with the sun in the A, or (1,0,0), direction (as viewed from the object). Calculations were also made for different sun directions for some objects, and eclipse response (no sun) was calculated for reference. The eclipse equilibrium potential indicates the equilibrium potential of a shadowed insulating cell.

In what follows, the term, "cell" is used to refer to a surface cell of a NASCAP object. A cell is one of the small square, rectangular, or triangular areas of exposed surface illustrated in figures 3 to 7. The "mesh size" is the length of one side of a square surface cell.

Object 1 (fig. 3) is an ATS-5 model object. It is an octagon with cavities on both ends, and with a smaller octagon rising one cell above the floor in each cavity. It has a two-cell wide metal belly band, and exposed metal patches scattered about the exterior surface. The charging of this object was calculated for both types of stabilization (spinning and 3-axis). Calculations were made for a "small" object of overall length 1.6 m and a "large" object of overall length 8.0 m. In addition to the sun direction +c, represented (1,0,0), a sun direction of (1,0,1) was used for some runs.

Object 2 (fig. 4) is identical to object 1 except that it has no cavities. Thus it is a solid octagon with a two-cell wide exposed metal belly band and scattered patches of exposed metal around the sides. The ends of the octagon are insulating. Charging calculations were made for this object for both stabilization types and for sun directions of (1,0,0)

and (1,0,1). Results are compared to those of object 1 to identify the impact of end cavitieson charging response (see Results section below).

Object 3 (fig. 5) is an octagon with a four-cell wide belly band, but with no scattered patch-es. Its purpose was to identify effects of the wider exposed metal area. Its charging response was calculated for the two stabilization types, with the sun in the +A direction.

Object 4 (fig. 6) is object 3 with a second octagon on a short boom added to represent an antenna. Its purpose was to identify the effect of a despun antenna on the charging response of a spinning body. Figure 6 indicates three different insulators. In fact these differ only in photoelectron current density emitted. In order to simulate properly a despun antenna in the NASCAP calculation, the photoemitted current density of the permanently shaded portions of the antenna was set to zero (insulator 2), and that of the constantly illuminated side (insulator 3) was set to 3.31 na/cm^2 so that in the averaging done during spin simulation, its effective photoemitted current density is 1 na/cm^2, the nominal value for the insulator used as the basis in all runs ("INSULATOR"). The charging response of this object was calculated with the body spinning and the antenna despun. Two sun directions were used, (1,0,0) and a slightly oblique one, (0.986,0,0.164). The latter sun direction was used to indicate local differential charging effects near the antenna.

Object 5 (fig. 7) is the "extended geometry" object. It consists of a central octagon with two rectangular paddles attached by short booms. Charging response of this object was calculated only in the 3 axis stabilized mode. It was sized so that the octagonal body was approximately the same size as the octagonal bodies of the "small" Object 1, and Object 2 through 4, and its overall Z dimension is comparable to that of the "large" Object 1. Its purpose was to identify effects of extended geometry (as compared to the compact octagonal geometry) on charging response.

B. Results

As a baseline, calculations of charging in eclipse were made. Each of the modeled objects charged to the equilibrium potential of -5.32 kV within a few seconds. The sunlight charging calculations were run for 30 minutes each. The largest negative potential developed by a shaded surface cell on any object was -2.3 kV, or about half its equilibrium potential. Thus the first general result is that sunlight charging is predicted to be a much slower process than eclipse charging. On the other hand, the structures of all objects did charge in sunlight to negative potentials of hundreds of volts during the 30 minutes of charging simulation. This is of particular interest because the plasma electron current density to an uncharged surface was more than an order of magnitude smaller than the photoelectron current density! The charging of the structure and sunlit insulation to negative potentials is thus not due to plasma electron fluxes exceeding photoelectron fluxes. Rather, it is a con-sequence of differential charging. Shaded insulating surfaces develop negative charges and set up potential barriers around the objects. These potential barriers make it impossible for photo-electrons to escape from the vicinity of the object, effectively cutting off photoelectron emission from sunlit cells, both metal and insulating, and allowing charging of the entire object. Thus sunlight charging is essentially a differential charging effect. Sunlight charging is expected to occur slowly be-cause the large capacitance of thin insulation to underlying conductors causes differential charging to occur slowly.

In the balance of this section, the three con-figuration features investigated are discussed in the order in which they appear in table II, that is effects of stabilization type (including effect of the despun antenna), effects of size, and finally, effects of geometry. A final paragraph summarizes the relative importance of these features in deter-mining overall charging response.

Calculations of the charging responses of Objects 1, 2, and 3 were made for each object spinning and 3-axis stabilized. Results indicate that type of stabilization is a very important factor in determining charging response. Predictions for Object 1 are shown in figure 8. As can be seen from the figure, the structure of the 3-axis stabilized object begins to charge sooner, after 2 to 3 minutes compared to 5 to 6 minutes for the spinning version. After 30 minutes, the structure potential in the 3-axis stabilized case is about three times that in the spinning case. The behavior of the shaded insulation in the two cases is interesting. During the first minute or two of charging (before the structure begins to charge negatively), dark insulation in the two cases charges at the same rate. The rate increases in each case after the structure begins to charge negatively, but the rates are such that the electric field inside the shaded insulation increases somewhat more quickly for the spinning than the 3-axis stabilized case. After 30 minutes of charging, there is about a 10% difference in electric field across shaded insulation in the two cases. For example, for the case illustrated

in figure 8, the field across dark insulation after 30 minutes of charging is 9.8X106 V/m in the spinning case compared to 9.1x106 V/m in the 3-axis stabilized case.

This appears to result from the larger proportion of shaded cells in the 3-axis stabilized case, and the consequently smaller region over which the potential barrier must extend to suppress photo-emission from all sunlit cells. Potential contours around Object 2 after 11 minutes of charging are shown in figure 9 for the 3-axis stabilized case and in figure 10 for the spinning case. In these figures, Qs is the structure potential, 601 is the potential of the shaded insulating cells, and 4sx is the potential of a sunlit insulating cell near the belly band. In general, sunlit insulating cells were found to be less negative than the structure. Because there are larger areas of exposed insulator than of exposed metal on all these objects, the formation of potential barriers which cut off photoemission from sunlit insulating cells is critical in allowing the structure to charge negatively.

The effect of the despun antenna (Object 4) on overall charging behavior was to increase the charging rate slightly over that for Object 3, which is identical except for the presence of the antenna on Object 4. Results are illustrated in figure 11. The antenna on Object 4 is small relative to the main body of this object. Presumably, if the relative size of the antenna were larger, its effect on the charging rate would be greater. It should be noted that, while the antenna's effect on the over-all charging of the object is small, its presence gives rise to large local differential charging between its shaded side and nearby cells on the top of the body, particularly when the sun is in a direction such that the top surface of the body is illuminated.

Results of charging response calculations for the large and small versions of Object 1 were compared to identify effects of overall size. Figure 12 shows these results for the 3-axis stabilized case. As the figure indicates, a factor of 5 change in linear dimensions caused at most a few percent change in charging response. This is a consequence of the fact that differential charging is' the dominant factor in sunlight charging.

Three types of geometry features were considered. These were: (1) compact versus extended; (2) end cavities; and (3) distribution of exposed metal.

To compare compact to extended geometry, the charging response of the large version of Object 1 was compared to that of Object 5. Object 1 is essentially an octagon, and represented a compact geometry. Object 5 is an octagon with large flat "wings," and is therefore considered extended. Figure 13 shows the comparison. Object 1 results shown are for the 3-axis stabilized condition. As can be seen from the figure, the extended object charges significantly more quickly. Its structure potential is about 1.5 times that of the compact object after 30 minutes of charging. The stress across shaded insulation at that point is somewhat larger for the compact object (9.1X106 V/m) than for the extended one (8.6X106 V/m). This is similar to the result for type of stabilization in that the object whose structure charges more quickly has lower stresses across its shaded insulation.

The effect of end cavities on charging response was examined by comparing results of charging calculations for Object 1 with those for Object 2. As noted above, these objects are identical except that Object 1 has end cavities and Object 2 does not. Results of the comparison indicate essentially no effect on overall charging response, that is, the potential versus time plots for the two objects' structures and shaded surfaces are virtually identical. This was true for both spinning and 3-axis stabilized cases, and for sun directions of (1,0,0) (+#c) and (0.707,0,0.707). In each case the (0.707, 0,0.707) sun direction resulted in slower charging but the results for Objects 1 and 2 were essentially the same for each combination of conditions (e.g., spinning, sun at (1,0,0), etc.). The fields in and near the cavities are strongly influenced by their presence, but the fields exterior to the objects, which form the photoelectron trapping barriers, are not much influenced by the presence of cavities. This is illustrated in figures 1 and 15. In figure 14 equipotential contours around Object 1 are shown after 20 minutes of charging in the spinning mode. Note the complicated field structures, particularly in the lower cavity, where the small octagonal "bump" in the cavity has a conducting circumferential surface. Figure 15 shows equipotential around Object 2 after 21 minutes of charging. A comparison of this figure to the previous one indicates that, despite the complex field structures in the cavities, the fields nearer the exterior surfaces of the two objects are very similar. Because these exterior fields, which suppress photoelectron emission, are the important ones in determining overall charging response, the two objects behave the same in terms of that response. It should be noted, however, that particularly in the oblique sun angle cases, severe differential charging occurs inside the cavities due to local shadowing effects.

Finally, the charging response of Objects 2 and 3 were compared to identify effects of distribution of exposed metal. The effect was slight enough (-5%) to be considered insignificant in this study. Object 3 charged slightly more slowly than Object 2, evidently because of differences in the details of potential barrier formation.

Results of the NASCAP configuration study are summarized in table III in terms of potentials on structures and dark insulation and stresses across the insulation after 30 minutes of charging simulation. Briefly, type of stabilization was the most important single factor in determining charging response. Overall geometry (extended versus compact) was second in importance. Other features investigated (size, cavities, and small despun antenna) had negligible effect on overall charging response, though severe local differential charging can be expected in cavities and around despun antennas.

IV. ATS-5 and ATS-6 Charging

The NASCAP study just described indicates that daylight charging should occur much more slowly than eclipse charging. Furthermore, a compact spinning object is expected to charge more slowly in sunlight than a large extended one, with the consequence that the small spinner should attain lower potentials for a given exposure time and environment. In terms of ATS-5 and ATS-6, the computer results lead to the expectations that (1) sunlight charging should occur much more slowly than eclipse charging, (2) differential charging (to the extent it can be inferred from the particle data) should accompany sunlight charging of the spacecraft structure and precede absolute charging, and (3) ATS-6 should charge more quickly than ATS-5 in a given environment. Because of the time and distance separations of the two spacecraft, direct comparison of responses to the same environment is not possible. However, expectation 3 also implies that ATS-6 should charge more frequently and to larger potentials than ATS-5, assuming that the general features (such as plasma temperatures plus time scales for changes) of the environments seen by the two spacecraft are similar. Based on the statistical results noted earlier (2) this assumption seems reasonable to within a factor of 2.

With the three expectations itemized above in mind, ATS-5 and ATS-6 data were examined with particular attention to time history of daylight charging events, evidence of differential charging, and frequency and level of charging for ATS-5. It was felt that the work reported in reference 3 gave a good estimate of frequency and level of daylight charging for ATS-6.

A. ATS-6 Results

To establish a baseline for comparing time histories of charging in eclipse and in sunlight, an injection of kilovolt plasma occurring in eclipse was sought. Such an event occurred on April 1, 1975 (day of year 91 of 1975). The particle data from the UCSC North-South detector for this event is shown in spectrogram format in figure 16. The spectrogram is essentially an energy versus time plot for electrons (top) and ions (bottom), with count rate of particles arriving at the detector indicated by intensity. The relationship of count rate to intensity is indicated by the grey scale to the right of the energy-time plot. In general, low count rates result in dark areas, and high count rates are indicated by bright areas. For a more de-tailed description of this format, see reference 7.

On day 91 of 1975, ATS-6 entered eclipse at 0549 UT (universal time). This is reflected in the particle data by the reduction in count rate of low energy electrons at that time. These low energy electrons are photoelectrons trapped by a potential barrier around the spacecraft.(7) At about 0625, an injection event occurred. The spacecraft responded by charging quickly to about -2000 V, as indicated by the change in the ion spectrum. The bright band of ions represents low energy ions accelerated through the spacecraft's potential, and thus indicates the spacecraft's potential. The time history of the spacecraft's potential during this event is shown in figure 17 on a linear scale. This figure shows clearly the almost immediate charging response when the injection occurred. Within a minute, the spacecraft potential changed from near zero to about -2000 V. Thus, as anticipated, eclipse charging occurs quickly.

Daylight charging of ATS-6 occurs quite frequently; the spacecraft was observed to be charged more than 50% of the time in the midnight to dawn local time quadrant.(3) A review of spectrograms of daylight charging events indicates two features in agreement with expectations. First, daylight charging occurs slowly. Times of 15 to 60 minutes for the charging transient are typical. Second, daylight charging events are accompanied by changes in the height of the potential barrier around the spacecraft, which is reflected in changes in the low energy electron spectra. The barrier becomes higher just before charging of the structure commences, and remains high during charging events. A collection of spectrograms, many of which show day-light charging of ATS-6 is published in reference 9.

An example of daylight charging response is shown in figure 18 in spectrogram format. Shown are data from the North-South detector on July 22 of 1974 (day of year 203 of 1974). An injection occurred at about 0740 UT. The boundary of the bright band of low energy electrons, indicating the height of the potential barrier, increases in energy, and the spacecraft potential (indicated by the bright rim of ions) goes negative to about -340 V, with discernable slope, even in the 24-hour spectrogram. Figure 19 shows the barrier height and spacecraft potential on a linear energy scale during this event. As can be seen from the figure, the barrier height increases to about 50 V several minutes before charging of the structure begins; the barrier height rises to about 100 V and is maintained at about that level during most of the event. The structure potential becomes negative relatively slowly, reaching about -340 V after some 40 minutes of charging. The electron temperature of the environment calculated from

$$kT_e = \text{Energy flux}/ 2 \text{ particle flux} \qquad (1)$$

was constant during this time period; from 0900 to 1000, the spacecraft potential decreased approximately linearly with the decreasing electron temperature.(10) Thus ATS-6 charges much more slowly in sunlight than in eclipse, and sunlight charging is accompanied by differential charging, as indicated by the increase in the height of the potential barrier.

B. ATS-5 Results

ATS-5 spectrograms for the period July 1969 through June 1971 were reviewed to identify day-light charging events. A total of 45 such events were found. Durations ranged from about 10 minutes to about 4 hours. The most negative potential re-corded was -400 V. Distributing the events in 15-minute segments of local time indicated that day-light charging for ATS-5 occurs mostly in the mid-night to dawn local time quadrant. This is similar to the ATS-6 case. However, for ATS-5, daylight charging occurred only about 2% of the time, even in this quadrant. Allowing for the fact that the ATS-5 particle detectors cannot detect charging of magnitude less than 50 V, and that about half the ATS-6 daylight charging events were to potentials of less magnitude than this, ATS-6 was charged to >50 V about 20% to 25% of the time in that local time quadrant, compared to the 2% for ATS-5. Clearly, ATS-5 charges less frequently, and to smaller potentials than does ATS-6.

Differential charging on ATS-5 is evidenced by a cutoff of the low energy electron data in the parallel detector. (11) The parallel detector is inside one of the cavities on ATS-5 (see fig. 1) looking parallel to the cylinder axis. This cutoff was first identified as a charging effect by DeForest.(4) In the review of ATS-5 data it was observed that day-light charging of this spacecraft was always pre-ceded and accompanied by this signature in the low energy electron data taken by the parallel detector. Figure 20 shows data from this detector on day 327 of 1970 (Nov. 23). At about 0600 UT the environment gradually becomes more active; starting at about 0630, the cutoff of low energy electrons be-comes evident as a reduction in the spectrogram's intensity. The energy edge of this cutoff rises slowly until about 1000, then gradually falls to zero by about 1700. The bright band of ions indicating spacecraft potential also appears in this data, but it is more easily seen in the data from the perpendicular detector, which is not complicated by local charging effects in the cavity. The perpendicular detector data for this event is shown in figure 21, again in spectrogram format. This figure shows that the spacecraft was charged to more than 50 V negative from about 0720 to 1200 on this day. The energy edge of the electron cutoff in the parallel detector and the spacecraft potential as determined from the perpendicular ion data are plotted on a linear scale in figure 22 for the time period 0700 to 1200. By 0700, the electron energy cutoff was about 500 eV; it reached about 750 eV before the spacecraft potential reached -50 V. The cutoff energy continued to increase as the spacecraft's negative potential increased, then began to fall off as the spacecraft's negative potential decreased to below 50 V at the end of the event. This was one of the longest daylight charging events for ATS-5; the most negative spacecraft potential recorded during the event was -390 V, around 1000. Its basic characteristics, however, are typical of ATS-5 charging events.

V. Summary and Conclusions

A computer study using the NASCAP code was performed to identify the basic characteristics of daylight charging, and the importance of various configuration features in determining daylight charging response. ATS-5 and ATS-6 flight data were examined to determine whether the computer predictions were supported by flight data.

Findings of the computer study were that day-light charging is essentially a differential charging effect. In consequence, daylight charging is expected to occur much more slowly than eclipse charging, and be accompanied by evidence of differential charging. A conclusion to be drawn here is that a spacecraft with completely conducting surfaces is unlikely ever to experience daylight charging.

Because daylight charging occurs so slowly, calculation of equilibrium potentials for a given set of environmental conditions will not give an accurate indication of charging response. It is unlikely that the environment will remain constant long enough for equilibrium to be reached. Also, because daylight charging response is dominated by the effect of potential barriers which suppress photoelectron emission, any calculation of response which does not account for such barriers will give incorrect results. Therefore, prediction of day-light charging response requires multidimensional, time-dependent calculations.

Configuration features important to daylight charging response were type of stabilization and overall geometry. Size, cavities, and presence of a small despun antenna had little effect on overall charging response, although the latter two have significant impact on local differential charging. Their importance also could be increased in the presence of field aligned fluxes.

The ATS-5 and ATS-6 data are entirely consistent with the computer predictions. Daylight charging is slow, and is accompanied by differential charging. ATS-5 charges less frequently, to lower potentials and probably more slowly than ATS-6. An interesting aspect of the daylight charging of ATS-5 is that no charging has been observed during the summer months (ref. 4 and this review of data). DeForest(4) suggested the possibility of some environmental difference at the ATS-5 orbital location. The present study indicates another possible reason: perhaps the cavity on the end opposite to the parallel detector has mostly conductive inside surfaces, so that no differential charging can occur there. Given that absolute charging of ATS-5 was always accompanied by evidence of differential charging in the parallel detector, the latter explanation seems quite plausible.

References

1. Purvis, C. K., Bartlett, R. 0., and DeForest, S. E., "Active Control of Spacecraft Charging on ATS-5 and ATS-6," in Proceedings of the Spacecraft Charging Technology Conference, C. P. Pike and R. R. Lovell, eds., AFGL-TR-77-0051 and NASA TM X-73537, Feb. 24, 1977, pp. 107-120.

2. Garrett, H. B., Mullen, E. G., Ziemba, E., and DeForest, S. E., "Modeling of the Geosynchronous Orbit Plasma Environment - Part 2, ATS-5 and ATS-6 Statistical Atlas," AFGL-TR-78-0304-PT-2, Nov. 30, 1978.

3. Reasoner, D. L., Lennartsson, W., and Chappell, C. R., "Relationship Between ATS-6 Spacecraft Charging Occurrences and Warm Plasma Encounters," Spacecraft Charging by Magnetospheric Plasmas, Progress in Astronautics and Aeronautics, vol. 47, A. Rosen, ed., AIAA, New York, 1976, pp. 89-101.

4. DeForest, S. E., "Spacecraft Charging at Synchronous Orbit," Journal of Geophysical Re-search, vol. 77, Feb. 1972, pp. 651-659.

5. Bartlett, R. O. and Purvis, C. K., "Summary of the Two Year NASA Program for Active Control of ATS-5/6 Environmental Charging" in space-craft Charging Technology - 1978, NASA CP 2071, 1979, pp. 44-58.

6. Katz, I., Cassidy, J. J., Mandell, M. J., Schnuelle, G. W., Steen, P. G., and Roche, J. C., "The Capabilities of the NASA Charging Analyzer Program," in Spacecraft Charging Technology - 1978, NASA CP 2071, 1979, pp. 101-122.

7. DeForest, S. E. and Mcllwain, C. E., "Plasma Clouds in the Magnetosphere," Journal of Geophysical Research, vol. 76, June 1, 1971, pp. 3587-3611.

8. Whipple, E. C., Jr., "Observation of Photo-electrons and Secondary Electrons Reflected From a Potential Barrier in the Vicinity of ATS 6," Journal of Geophysical Research, vol. 81, Feb. 1, 1976, pp. 715-720.

9. Garrett, H. B., McInerney, R. E., DeForest, S. E., and Johnson, B., "Modeling of the Geosynchronous Orbit Plasma Environment - Part 3. ATS-5 and ATS-6 Pictorial Data Atlas," AFGLTR-79-0015-PT-3, Jan. 15, 1979.

10. Johnson, B., Quinn, J., and DeForest, S. E., "Spacecraft Charging on ATS-6," Preprints of Proceedings of the 1978 Symposium on the Effect of the Ionosphere on Space and Terrestrial Systems, Naval Research Lab and Office of Naval Research, Washington, D.C., Jan. 24-26, 1978, Paper 4-10.

11. Synchronous Orbit Plasma Environment - Part 2, ATS-5 and ATS-6 Statistical Atlas," AFGL-TR-78-0304-PT-2, Nov. 30, 1978.

TABLE I. - SPACECRAFT CHARACTERISTICS SUMMARY

Launch (technology)	ATS-5 1969	ATS-6 1974
Attitude control	Spin stabilized	3-Axis stabilized
Exterior surface	Quartz, paint	Kapton, aluminum, quartz, silicon, paint
Characteristic dimension	2 m	10 m
Geometry	Cylindrical	Extended

TABLE II. – SUMMARY OF CONFIGURATION STUDY RUNS

Configuration feature	Comparisons made
Stabilization	Object 1: Spinning versus 3-axis stabilized Object 2: Spinning versus 3-axis stabilized Object 3: Spinning versus 3-axis stabilized Object 3: Spinning versus Object 4 (effect of despun antenna)
Size	Object 1: Mesh size = 0.1 versus mesh size = 0.5
Geometry	Large Object 1 versus Object 5 (compact versus extended) Object 1 versus Object 2 (effect of end cavities) Object 2 versus Object 3 (distribution of exposed metal)

TABLE III. - POTENTIALS AND STRESSES AFTER 30 MINUTES

Object number	Spinning			3-Axis stabilized		
	ϕ_S^a, V	ϕ_{DI}^b, V	Stress, V/m	ϕ_S^a, V	ϕ_{DI}^b, V	Stress, V/m
1	-380	-1360	9.8×10^6	-970	-1880	9.1×10^6
2	-390	-1360	9.7×10^6	-980	-1880	9.0×10^6
3	-310	-1330	1.0×10^7	-780	-1710	9.3×10^6
4	-370	-1350	9.8×10^6	-----	-----	-------
5	----	-----	-------	-1440	-2300	8.6×10^6

[a] ϕ_S = structure potential.

[b] ϕ_{DI} = potential of shaded insulator.

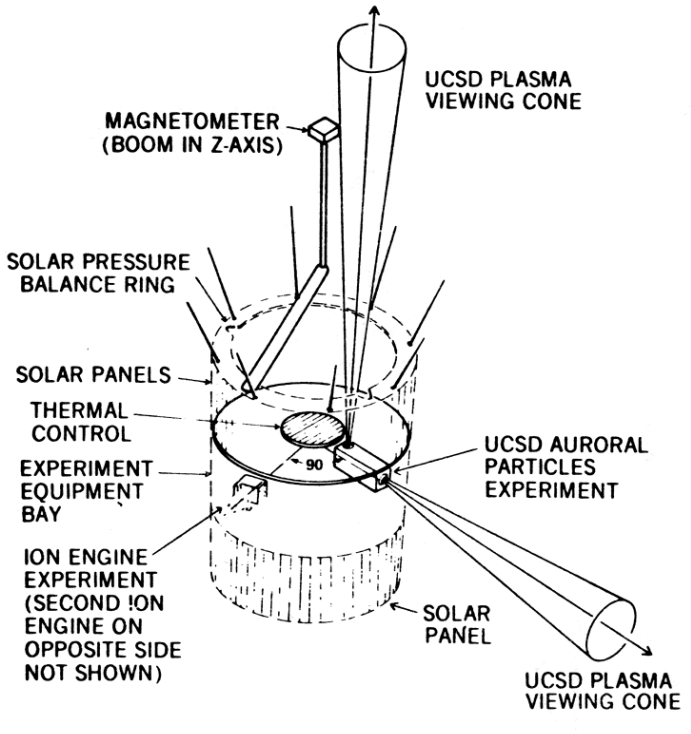

Figure 1. - ATS-5 orbital configuration.

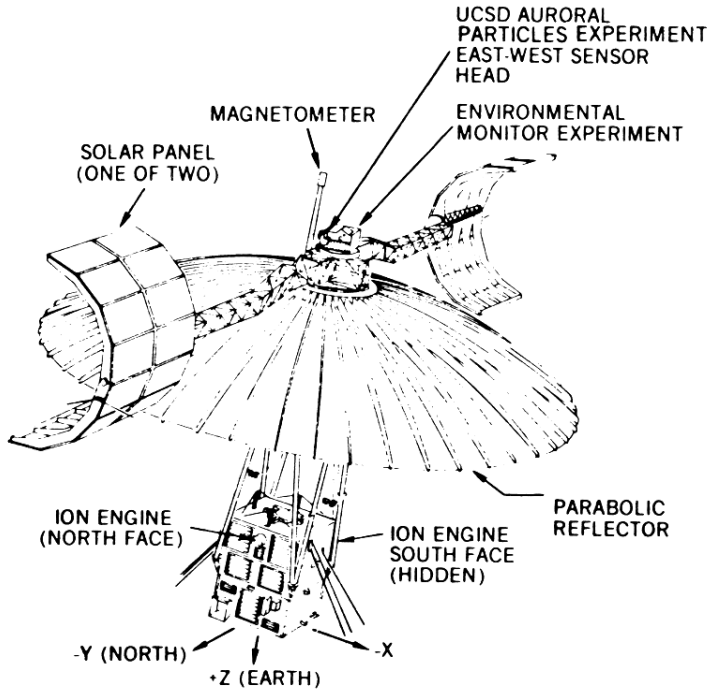

Figure 2. - ATS-6 orbital configuration.

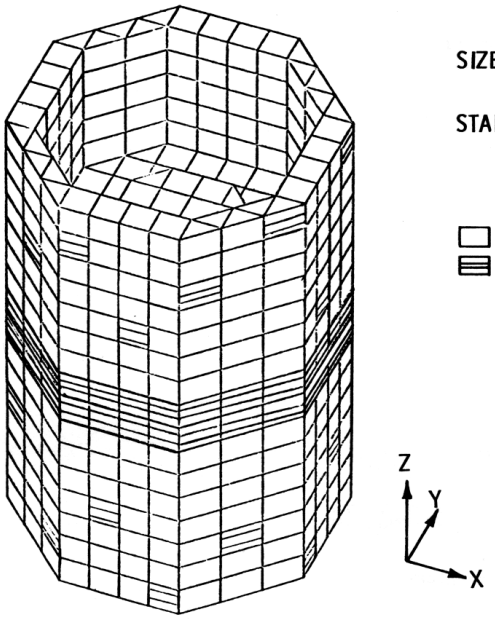

Figure 3. - Object 1 (ATS-5 model object)

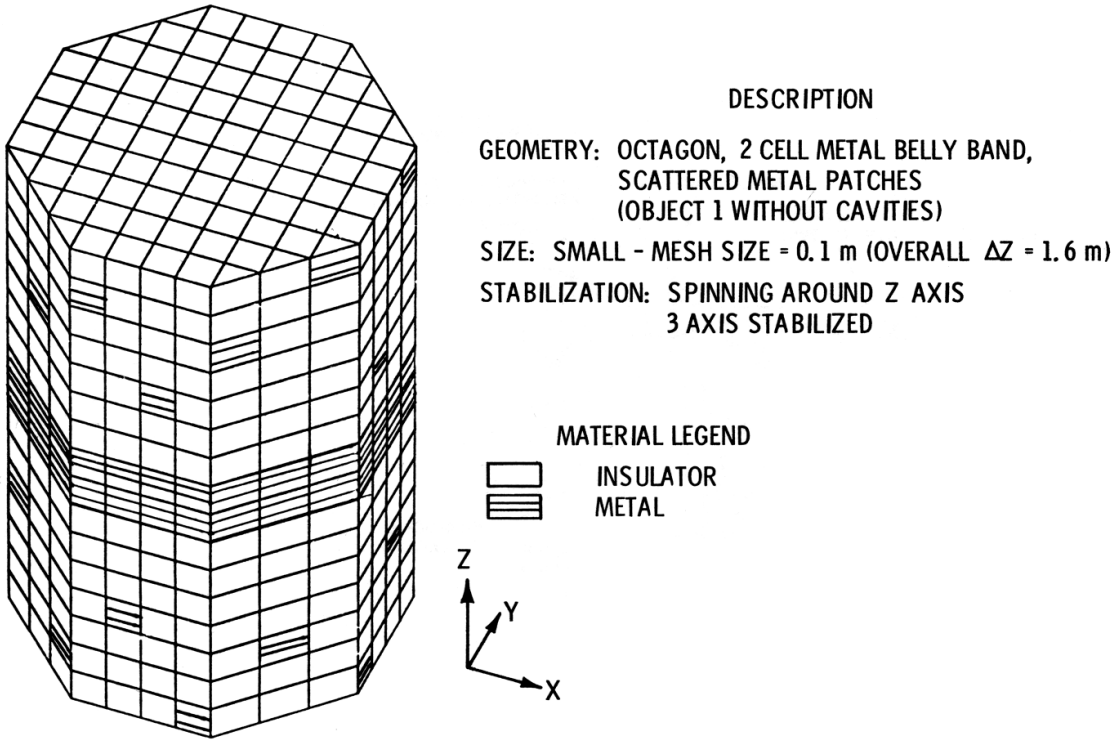

Figure 4. - Object 2.

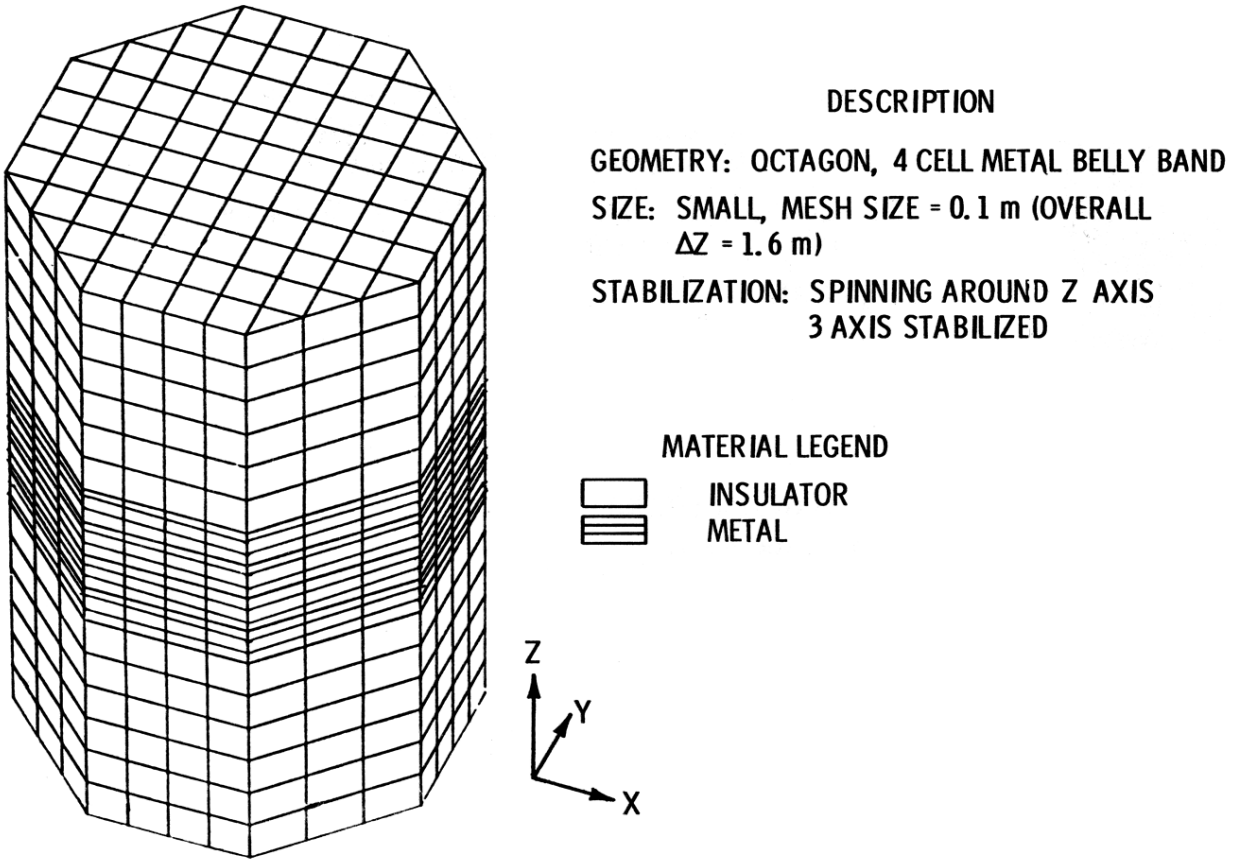

Figure 5. - Object 3.

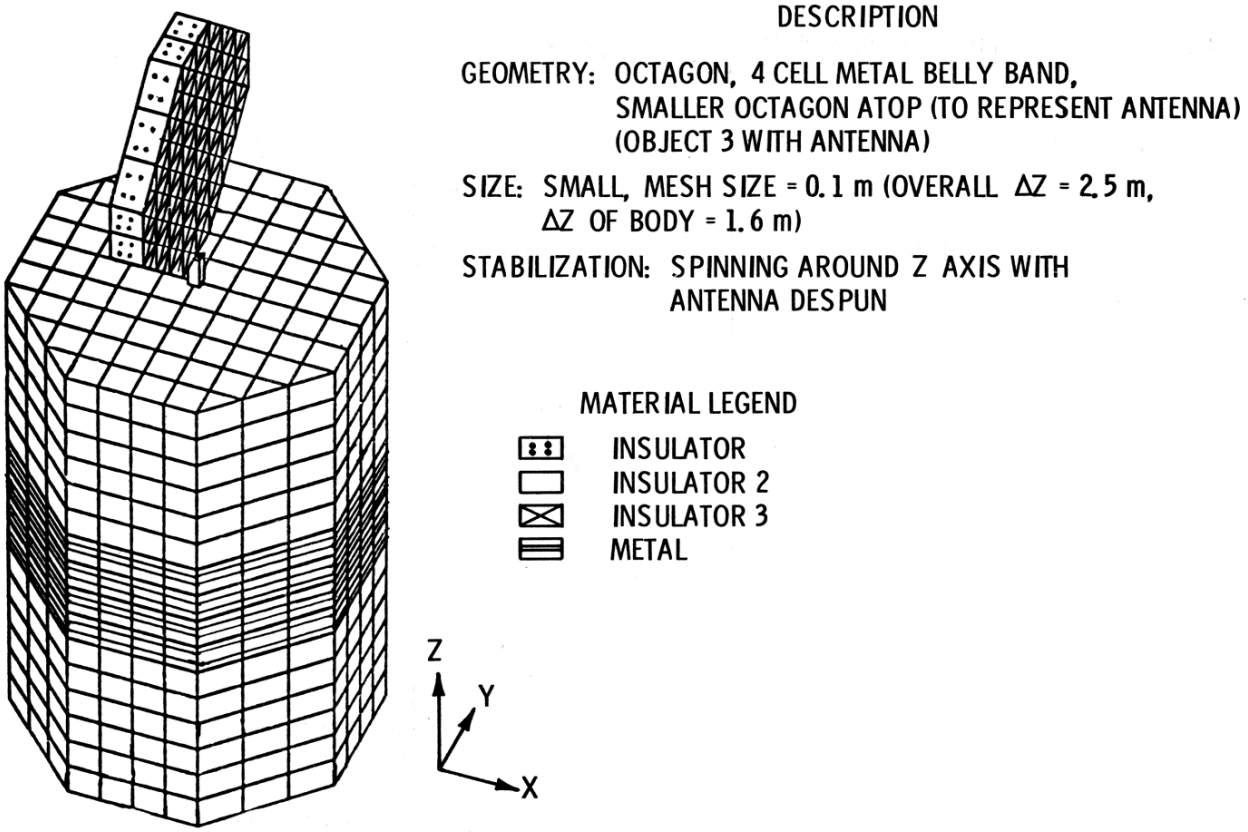

Figure 6. - Object 4.

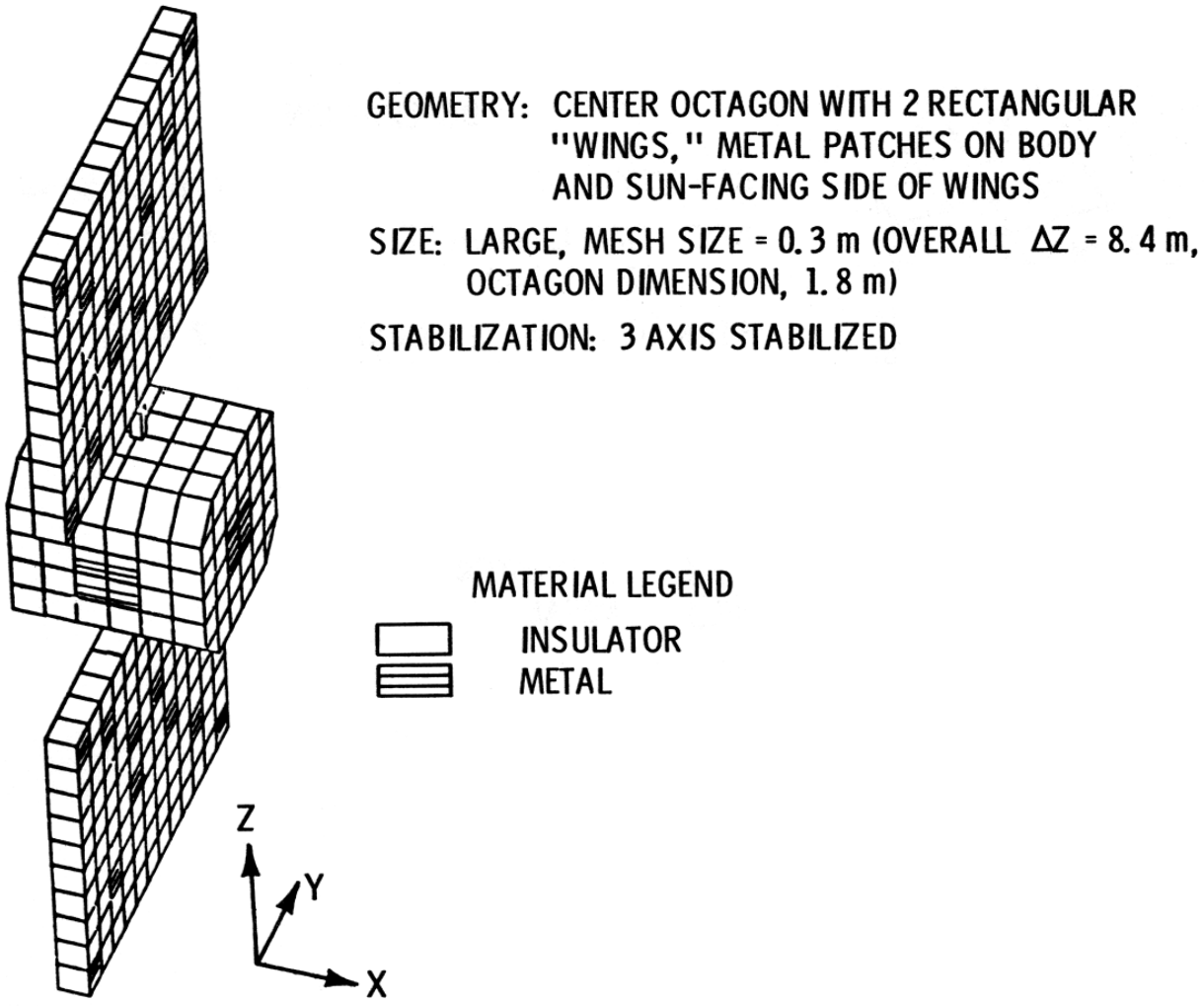

Figure 7. - Object 5.

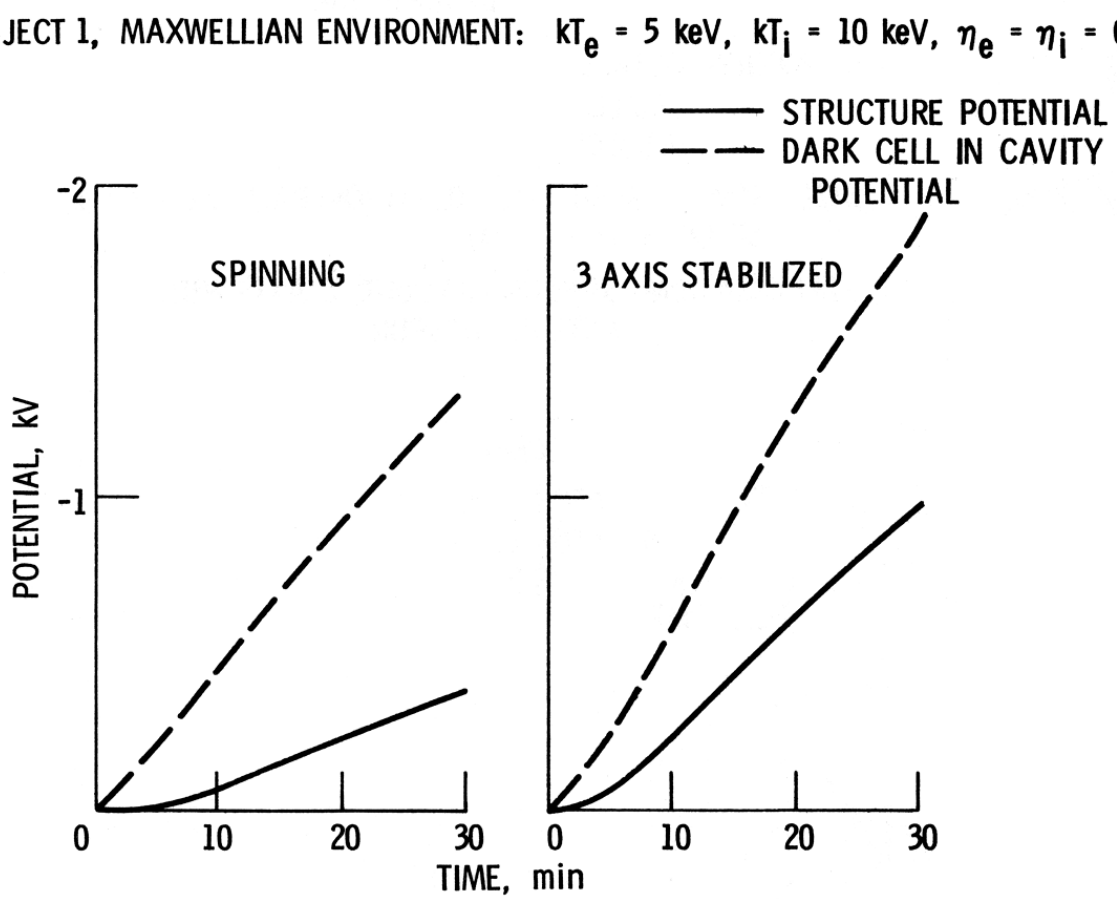

Figure 8. - NASCAP predictions: sunlight charging; effect of stabilization type.

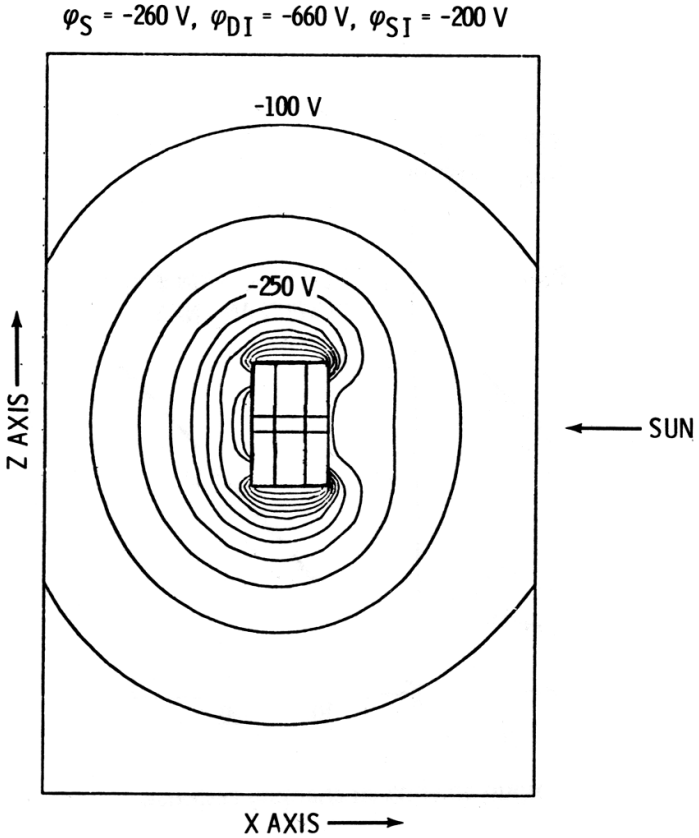

Figure 9. - Potential contours after 11 minutes of charging. Object 2, 3 axis stabilized.

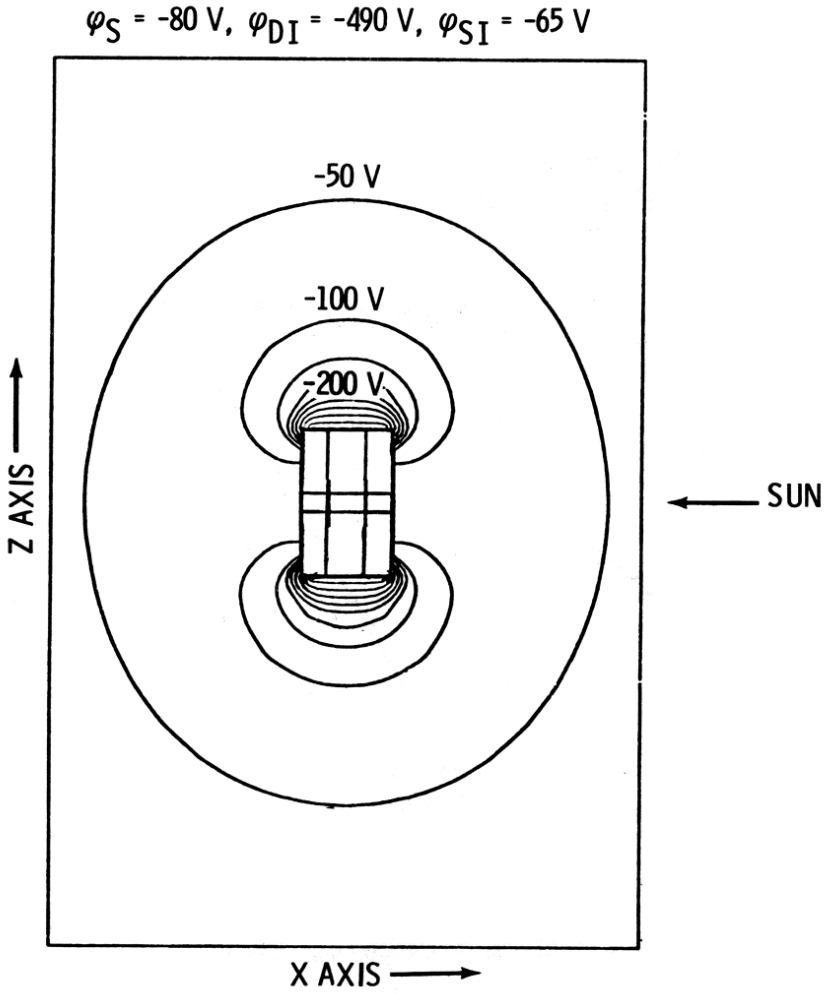

Figure 10. - Potential contours after 11 minutes of charging. Object 2, spinning.

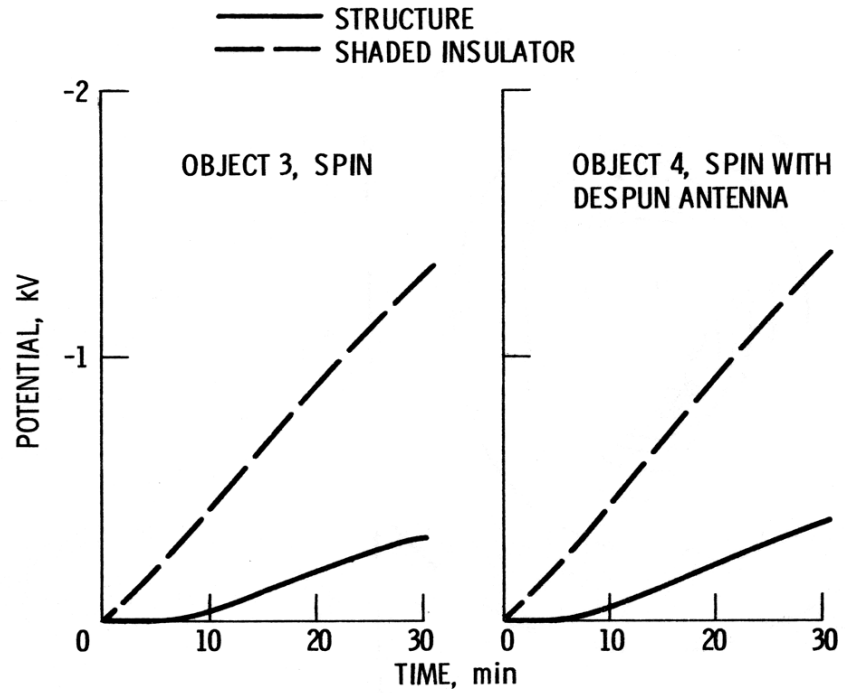

Figure 11. - Effect of despun antenna on charging response.

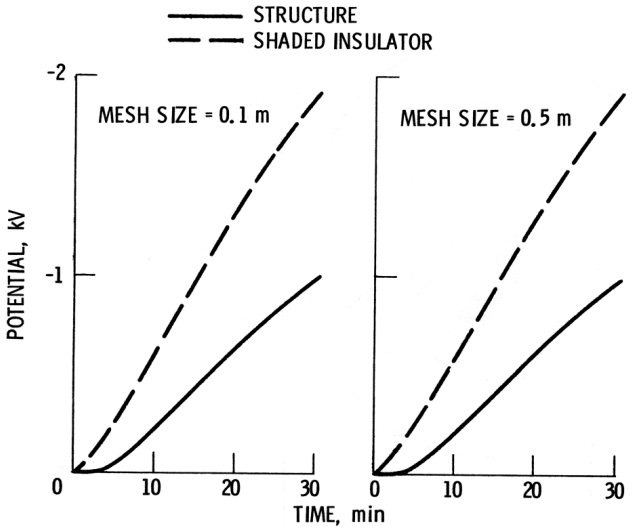

Figure 12. - Effect of size on charging response. Object 1, 3 axis stabilized. Sun at 1, 0, 0.
STRUCTURE - - SHADED INSULATOR
OBJECT 5, MESH SIZE = 0.3 m/ (EXTENDED)
OBJECT 1, MESH SIZE = 0.5 m (COMPACT)
/

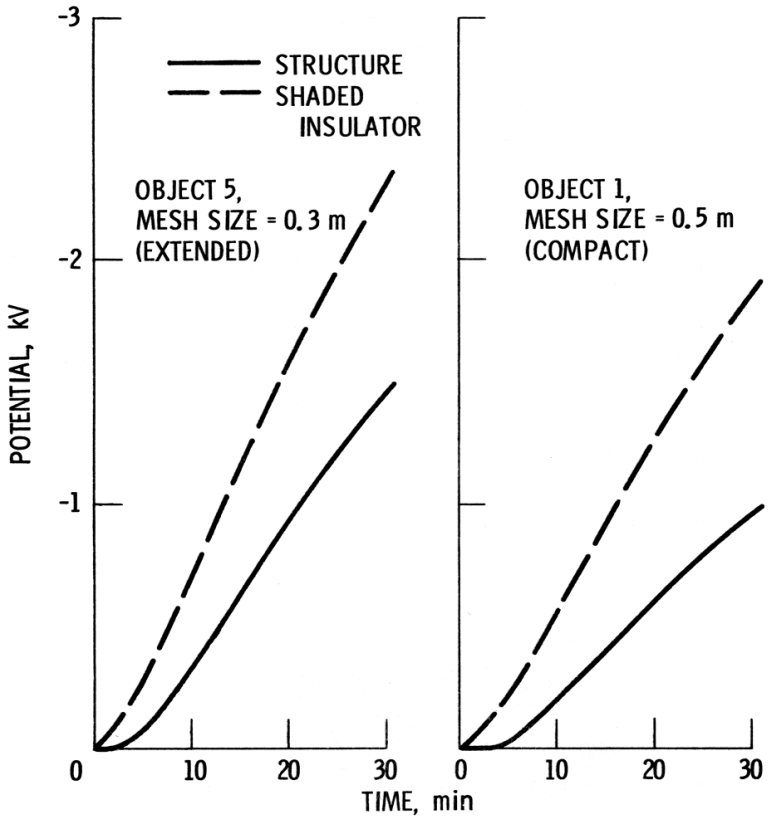

Figure 13. - Effect of geometry type on charging response.

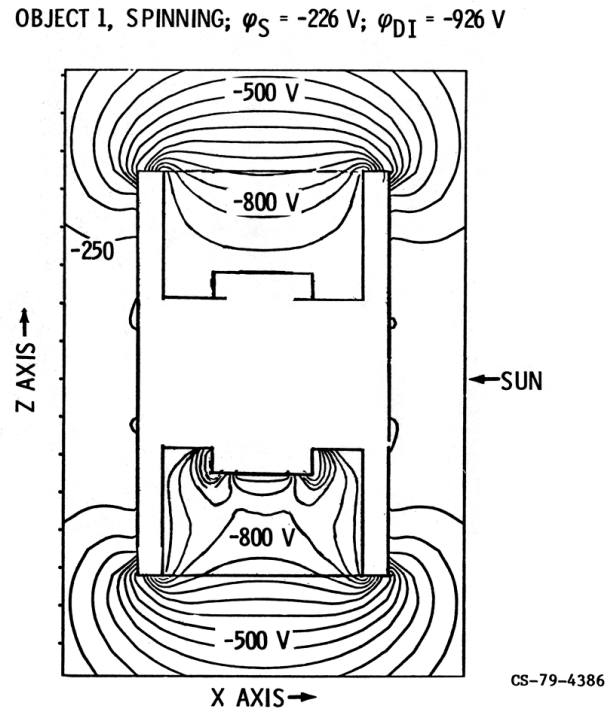

Figure 14. - Potential contours after 20 minutes of charging.

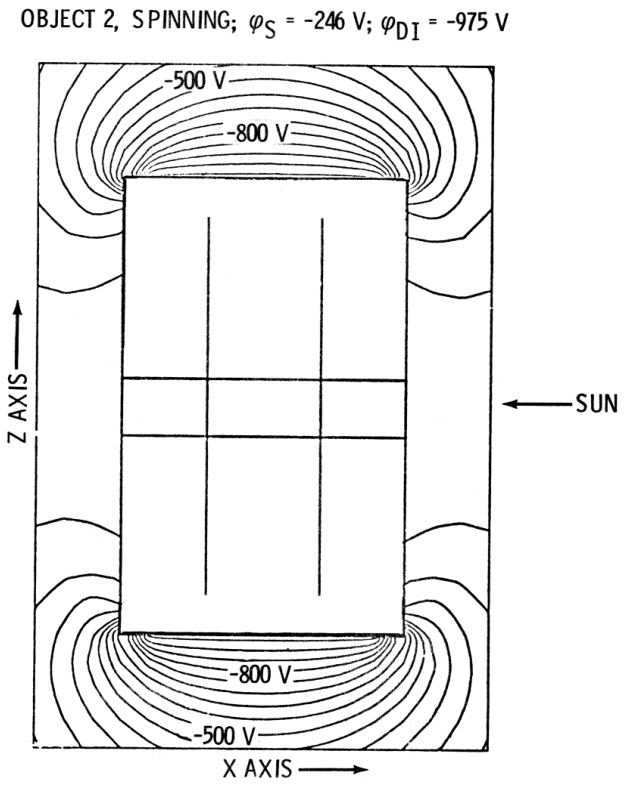

Figure 15. - Potential contours after 21 minutes of charging.

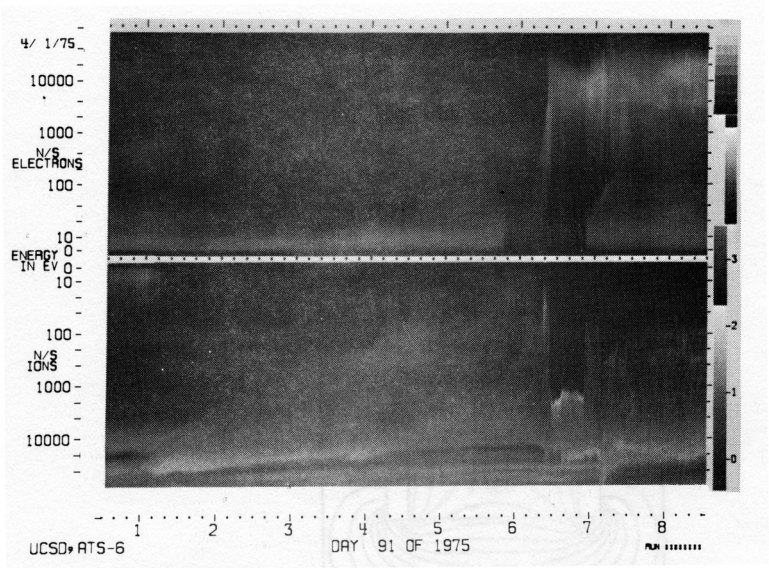

Figure 16.- ATS-6 spectrogram, day 91 of 1975: injection during eclipse.

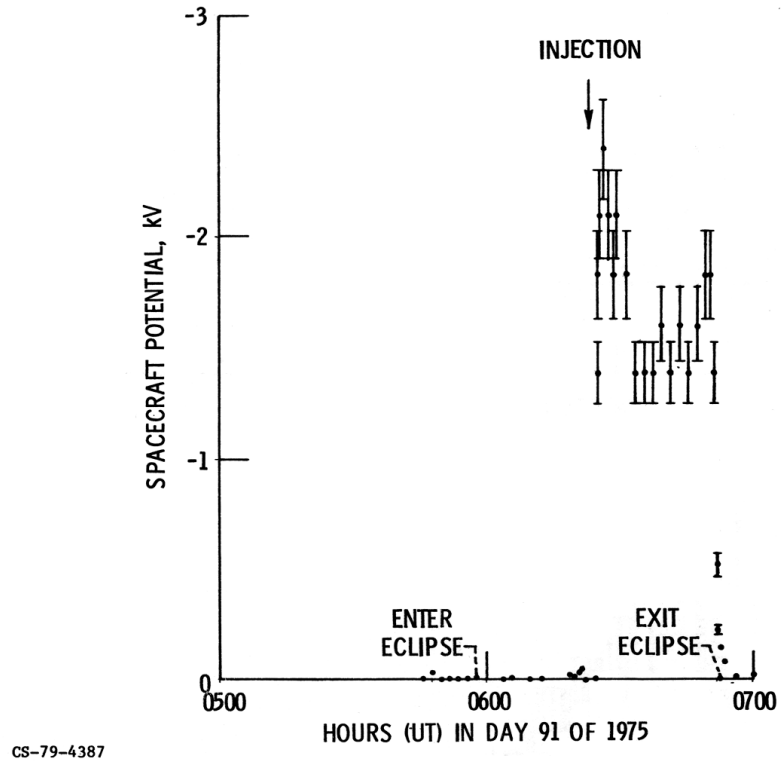

Figure 17. - ATS-6 potential: response to injection during eclipse.

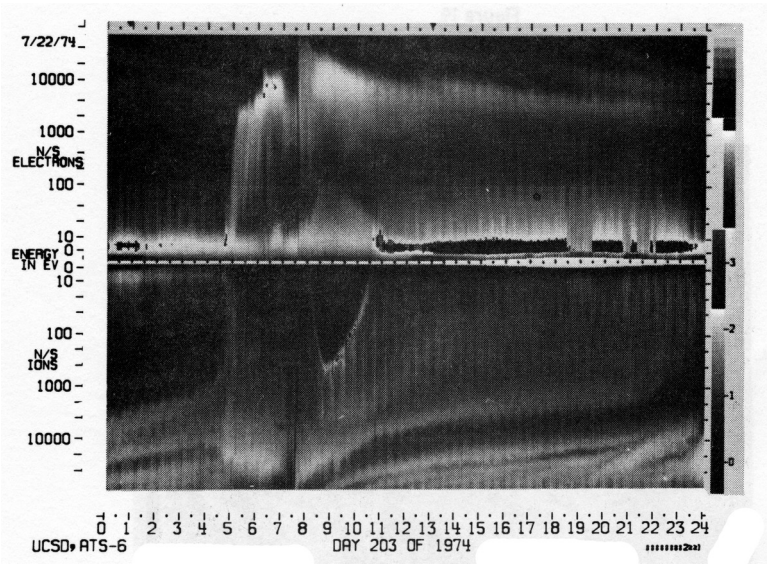

Figure 18.- ATS-6 spectrogram: daylight charging.

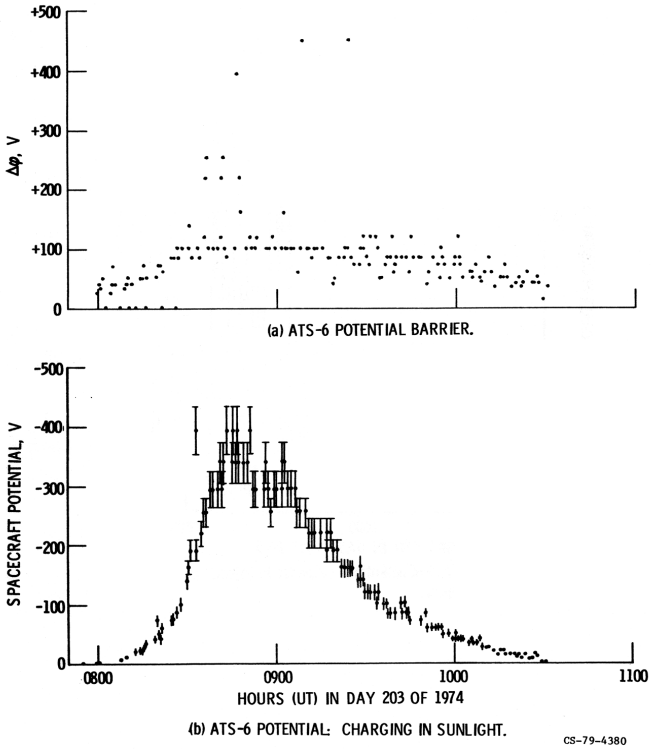

Figure 19.

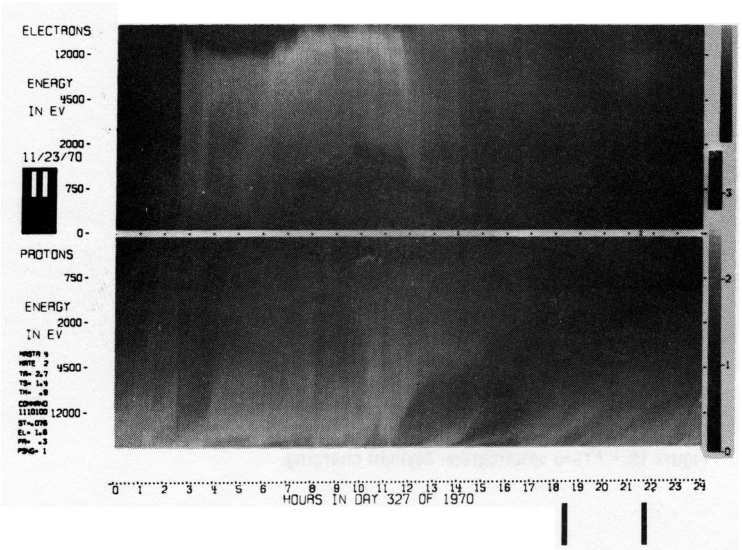

Figure 20.- ATS-5 daylight charging data, parallel detector.

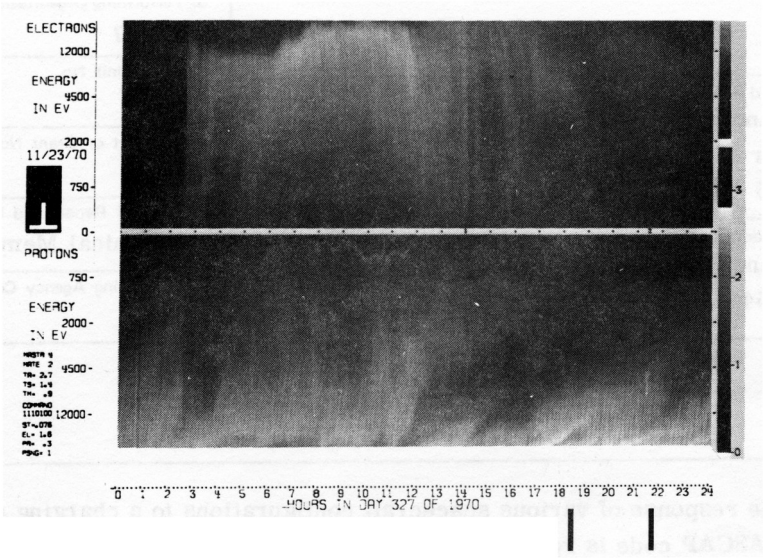

Figure 21.- ATS-5 daylight charging data, perpendicular detector.

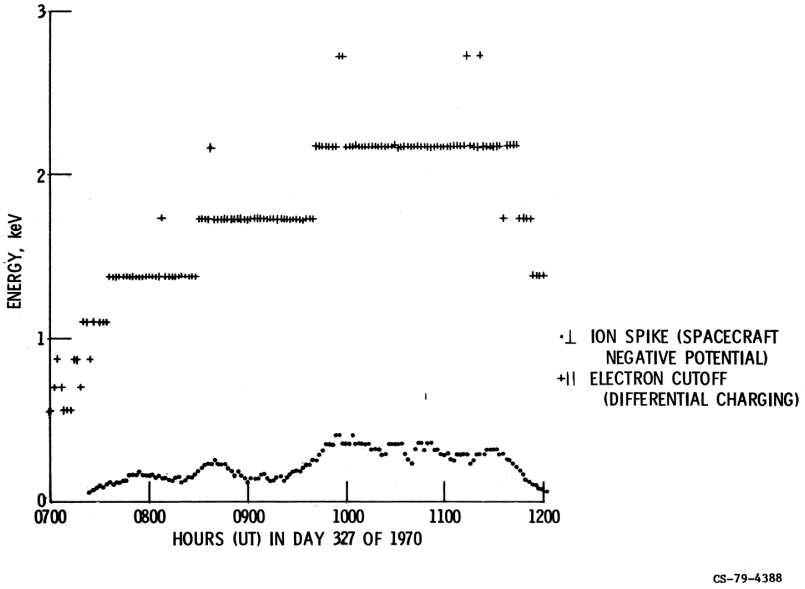

Figure 22. - ATS-5 data: charging in sunlight.